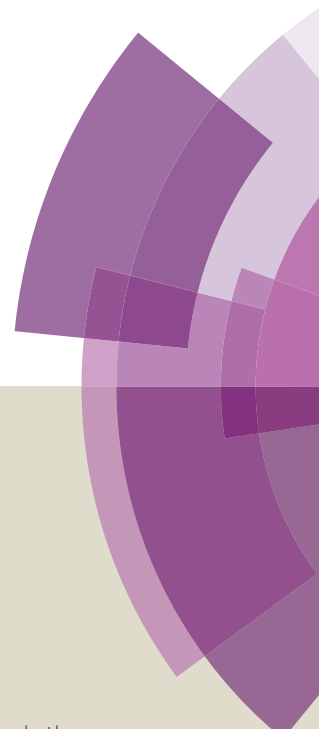


Journal of Materials Chemistry A

Accepted Manuscript



This article can be cited before page numbers have been issued, to do this please use: S. Zulfiqar, D. Mantione, O. El Tall, M. I. Sarwar, F. Ruipérez, A. Rothenberger and D. Mecerreyes, *J. Mater. Chem. A*, 2016, DOI: 10.1039/C6TA01457G.



This is an *Accepted Manuscript*, which has been through the Royal Society of Chemistry peer review process and has been accepted for publication.

Accepted Manuscripts are published online shortly after acceptance, before technical editing, formatting and proof reading. Using this free service, authors can make their results available to the community, in citable form, before we publish the edited article. We will replace this *Accepted Manuscript* with the edited and formatted *Advance Article* as soon as it is available.

You can find more information about *Accepted Manuscripts* in the [Information for Authors](#).

Please note that technical editing may introduce minor changes to the text and/or graphics, which may alter content. The journal's standard [Terms & Conditions](#) and the [Ethical guidelines](#) still apply. In no event shall the Royal Society of Chemistry be held responsible for any errors or omissions in this *Accepted Manuscript* or any consequences arising from the use of any information it contains.



Journal of Materials Chemistry A

PAPER

Nanoporous Amide Networks Based on Tetraphenyladamantane for Selective CO₂ Capture†Received 00th February 2016,
Accepted 00th February 2016

DOI: 10.1039/x0xx00000x

www.rsc.org/MaterialsA

Sonia Zulfiqar,^{a,b} Daniele Mantione,^b Omar El Tall,^c Muhammad Ilyas Sarwar,^{ad} Fernando Ruipérez,^b Alexander Rothenberger^e and David Mecerreyes^{bf}

Reduction of anthropogenic CO₂ emissions and CO₂ separation from post-combustion flue gases are among the imperative issues in spotlight at present. Hence, it is highly desired to develop efficient adsorbents for mitigating climate change with possible energy savings. Here, we report the design and facile one pot catalyst-free synthetic protocol for the generation of three different nitrogen rich nanoporous amide networks (NANs) based on tetraphenyladamantane. Besides the porous architecture, CO₂ capturing potential and high thermal stability, these NANs possess notable CO₂/N₂ selectivity with reasonable retention while increase in temperature from 273K to 298K. The quantum chemical calculations also suggest that CO₂ interact mainly in the region of the polar amide groups (–CONH–) present in NANs and this interaction is much stronger than with N₂ thus leading to better selectivity and affirming them as promising contenders for efficient gas separation.

Introduction

Climate change due to rising carbon dioxide (CO₂) level in the atmosphere is undoubtedly an issue of major concern.¹ It is crucial to mitigate anthropogenic CO₂ emissions from the environmental viewpoint for the remediation of CO₂ concentration in the atmosphere. Actual technological solutions involve the capture of CO₂ using liquid absorption, solid adsorption, membrane and cryogenic separations.² Owing to the easy handling and regeneration; solid adsorbents are generally more renowned, in particular focusing on physisorption as compared to energy intensive chemisorption processes. CO₂/N₂ selectivity is a parameter of

paramount importance together with gas uptake ability from practical CO₂ capture application perspective. One of the limitations associated with physisorption is the absence of chemical bond formation that leads to lack of CO₂ selectivity, although many attempts have been carried out to enhance selectivity by tuning the structure and introducing various functional groups, but often resulted in lowering of CO₂ sorption values. However, N₂ phobicity of materials and introduction of CO₂ philic groups can help in improving the CO₂ selectivity.^{2,3} Recently, porous polymer networks (PPNs),³ gained significant attention as gas adsorbents due to their facile synthesis, high physicochemical stability and surface area, low framework density and tunable porosity. Other well-known sorbents that have shown potential for CO₂ capture includes polymers of intrinsic microporosity (PIMs),⁴ covalent organic frameworks (COFs),⁵ conjugated microporous polymers (CMPs),⁶ hypercrosslinked polymers (HCPs),⁷ porous aromatic frameworks (PAFs)⁸ and others. It is established that the presence of numerous heteroatoms, in particular nitrogen and oxygen in combination with an intrinsic meso-nanoporosity in the polymer networks led to superior CO₂ capture ability owing to increased dipole–quadrupole interactions between the CO₂ molecules and polymer framework.⁹ Therefore, the curiosity in exploiting mildly basic amide functionality possessing binary interaction sites (N–H and C=O) for CO₂ capture is indeed of particular concern.

Aromatic polyamides belong to a class of high performance materials owing to their outstanding mechanical strength, thermal stability and chemical resistance.¹⁰ The structural rigidity and strong intermolecular hydrogen bonding developed via amide functionality results in dense chain packing thus rendering them ideal for spinning

^a Department of Chemistry, School of Natural Sciences (SNS), National University of Sciences and Technology (NUST), Islamabad 44000, Pakistan. Email: soniazulfiqar@sns.nust.edu.pk, soniazulfiqar@yahoo.com; Fax: +92 51 90855552; Tel: +92 51 90855608

^b POLYMAT, University of the Basque Country UPV/EHU, Jaxe Mari Korta Center, Avda. Tolosa 72, 20018 Donostia-San Sebastián, Spain.

^c Analytical Core Laboratories, King Abdullah University of Science and Technology (KAUST), Thuwal 23955-6900, Kingdom of Saudi Arabia

^d Department of Chemistry, Quaid-i-Azam University, Islamabad 45320, Pakistan

^e Physical Sciences and Engineering Division, King Abdullah University of Science and Technology (KAUST), Thuwal 23955-6900, Kingdom of Saudi Arabia

^f Ikerbasque, Basque Foundation for Science, E-48011, Bilbao, Spain.

† Electronic supplementary information (ESI) available: Detailed experimental section including synthetic procedures of the monomers and NANs, Reaction schemes, FT-IR spectra, CP/MAS ¹³C NMR spectra, BET linear plots, Cartesian coordinates of CO₂, N₂, NANs, NANs/CO₂ and NANs/N₂ complexes, Calculation methods, Isothermic heat of N₂ adsorption, IAST fitting curves and parameters. Comparison of CO₂ adsorption data and CO₂/N₂ selectivity with other porous polymers reported in literature. See DOI: 10.1039/x0xx00000x

into high performance fibers, tailoring bullet proof vests and flame-resistant garments. These polymers have well known industrial relevance predominantly in defense, automobile and aerospace applications.¹¹ CO₂ capture ability of organic amide polymers have rarely been studied so far with few exceptions.¹²⁻¹⁴

Cycloaliphatic hydrocarbons like adamantane possess a diamond-like cage structure. The most intriguing aspect of this tecton is its highly symmetrical tetrahedral shape along with huge molecular volume and stiffness rendering it a superb building block for generating supramolecular architectures. Adamantane structure consists of six secondary and four tertiary carbons. The hydrogens attached to the tertiary carbons can be readily converted into desired functional groups because of their high reactivity.¹⁵⁻¹⁷ The arylation of adamantane afford tetraphenyladamantane (TPA) consisting of adamantane core surrounded by four peripheral phenyl rings that can be easily functionalized and can spread out further.¹⁸⁻²² Shen and co-workers have synthesized TPA based microporous polycyanurate and polyimide networks and showed promising results for CO₂ adsorption.¹⁸ Li and fellow colleagues also thoroughly investigated the gas sorption properties of microporous poly(Schiff base) and polyaminal networks constructed from TPA.^{21, 22} The remarkable molecular structure of TPA also motivated us to synthesize amide networks exclusively from these units. The inclusion of bulky and stiff TPA moiety not only ensures the pore formation but also offer both cycloaliphatic and aromatic constituents in the NANs. To the best of our knowledge, this is the first ever report on the synthesis, characterization, gas sorption and CO₂/N₂ selectivity of nanoporous nitrogen rich amide networks based on tetraphenyladamantane. A series of amide networks have been synthesized by combination of TPA with di-, tri- and tetra functional aromatic units. Moreover, different factors affecting gas sorption properties such as chemical structure, nanoporosity, temperature and pressure were investigated. The quantum chemical calculations suggest that CO₂ interacts mainly in the region of polar amide groups present in the amide networks and this interaction is much stronger than N₂ resulting in noteworthy CO₂/N₂ selectivity. The CO₂ philic amide functionality of NANs provides high N-content whereas the presence of mesopores²³ also assists in the strong binding with CO₂ thus making NANs as promising contenders for post combustion CO₂ separations.

Experimental

Materials

2-Bromo-2-methylpropane(96%), 1-bromoadamantane (99%), potassium nitrate (99%+), acetic anhydride (99%+), glacial acetic acid (99.8%), palladium on activated carbon,10% Pd, unreduced, iodine (99.5%), copper cyanide (99%), [bis(trifluoroacetoxy)iodo] benzene (98%), N,N-dimethylformamide, anhydrous (>99.9%), dichloromethane, anhydrous (>99.8%) and oxalyl chloride (98%) were procured from Acros Organics. Anhydrous aluminium chloride (≥99.9%), benzene (>99%), triethylamine (≥99.5%), tetrahydrofuran, anhydrous (≥99.9%), sodium metabisulfite (≥99%), heptane (99%) and sodium sulphate, anhydrous (≥99.0%) were supplied by the courtesy of Sigma-Aldrich. Terephthaloyl chloride (≥99%) and trimesoyl chloride (98%) were obtained from Aldrich.

Hydrochloric acid (~37%), chloroform (99.8%), sulfuric acid (>99%), dimethyl sulfoxide (99.9%), i-pentane (>99%), potassium cyanide (>97%), ethylene glycol (>99.9%) acetone (>99%) and extra pure methanol were provided by Fisher Scientific. Potassium hydroxide (90%) was purchased from Scharlab and used as received.

Characterization methods

The elemental analysis of monomers and NANs was performed on a LECO CHNS-932 microanalyzer. Fourier transform infrared (FTIR) spectra were recorded over the range 4000–400 cm⁻¹ at a resolution of 4 cm⁻¹ using Bruker FTIR spectrometer Alpha-P. ¹HNMR measurements of the monomers were carried out on a Bruker AVANCE 400 spectrometer. The samples were dissolved in DMSO-d₆ and CDCl₃, and were measured with tetramethylsilane as an internal reference. Solid state NMR spectroscopic analysis of NANs was performed on a Bruker 400 AVANCE III WB spectrometer 9.40T. Cross-polarization magic-angle spinning (CP/MAS) ¹³C NMR spectra were recorded using a 4mm MASDVT probe at a spinning of 12 KHz, using the cross polarization pulse sequence, at 100.63 MHz, a time domain of 2K, a spectral width of 29 KHz, a contact time of 1.5ms and an interpulse delay of 5s. X-ray diffraction pattern of powdered NANs were recorded by a BRUKER D8 ADVANCE powder diffractometer at 40 kV and 30 mA. Measurements were performed for 2θ in the range of 2° to 80° with a step size of 0.05° and scan speed of 0.6°/min and scan time of 5s at 25°C. Thermogravimetric analysis (TGA) on NANs was performed using a TA instruments Q500 device. The samples were heated from room temperature to 800°C with a heating rate of 10°C/min under N₂ atmosphere with a gas flow rate of 10 mL/min. The surface morphology of NANs was determined using FEI Quanta 250 FEG and Magellan scanning electron microscope (SEM). NANs were also examined in a transmission electron microscope, TECNAI G2 20 TWIN (FEI), operating at an accelerating voltage of 200 kV in a bright-field image mode. Sample preparation for TEM involved the deposition of a solution drop on lacey carbon film copper grid which has previously been hydrophilized by a glow discharge process. To determine the porosity and Brunauer–Emmett–Teller (BET) surface area of NANs, N₂ adsorption isotherms at 77 K were obtained using Micromeritics ASAP 2020 physisorption analyzer. CO₂ and N₂ adsorption-desorption isotherms of NANs were recorded using Micromeritics ASAP 2050 sorption analyzer at 273K and 298K. The samples were degassed at 393K for 24h prior to analysis.

Synthesis of amide networks based on tetraphenyladamantane

Tetraphenyladamantane based three nitrogen-rich nanoporous amide networks (NAN-1, NAN-2 and NAN-3) were synthesized using one pot catalyst-free polycondensation reaction under basic conditions. The detailed step by step protocol for the synthesis and characterization of tetra-amine monomer 1,3,5,7-tetrakis(4-aminophenyl) adamantane (TAPA) and tetra-acid chloride monomer, 1,3,5,7-tetrakis(4-(chlorocarbonyl)phenyl)-adamantane (TCPA) is described in ESI (Scheme S1 and Scheme S2†). A typical synthesis of NANs involved the reaction of TAPA with terephthaloyl chloride (TPC), trimesoyl chloride (TMC) and TCPA (Scheme 1) in the presence of triethylamine (TEA) to quench the hydrochloric acid

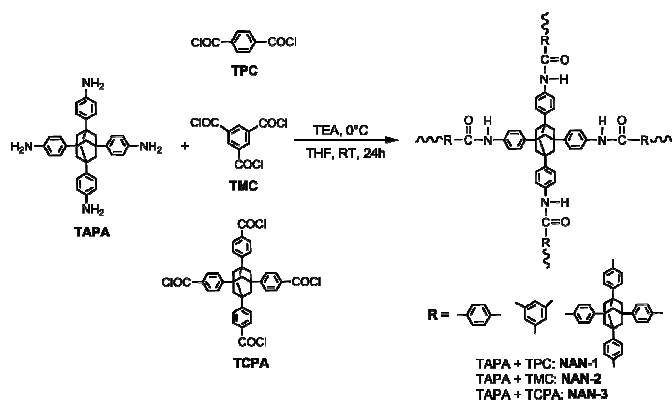
(HCl) generated as a by-product during the polymerization reaction in inert atmosphere. THF was used as a solvent medium for the synthesis of NANs and the reaction was carried out initially at 0°C to avoid any side reactions because the permanent porosity in polymer networks is very much reliant on the high conversion rate during the polymerization reaction. The stirring was continued at room temperature for 24h and afterwards the precipitates of NANs were collected by filtration and washed several times with THF, water, and acetone to remove hydrochloride salt and organic oligomeric impurities. The resultant NAN powders were then immersed in acetone for two days during which time the acetone was decanted and freshly replenished three times and dried under vacuum for 24h (see detailed procedure in the ESI†).

Computational Details

All the density functional calculations (DFT) have been carried out with the Gaussian 09 suite of programs.²⁴ The geometrical optimizations were performed using the long-range corrected functional ω B97XD,²⁵ which includes dispersion corrections, together with the 6-31+G(d,p) basis set. Harmonic vibrational frequencies were obtained, at the same level of theory, by analytical differentiation of the gradients in order to determine whether the structures were minima or transition states. All structures showed real frequencies for all of the normal modes of vibration. These frequencies were then used to evaluate the zero-point vibrational energy (ZPVE) and the thermal corrections, at T = 298 K, in the harmonic oscillator approximation. The electronic energy was refined by single-point calculations using the 6-311++G(2df,2p) basis set. The binding energy of gas (CO₂ or N₂) with the model of NANs was estimated as follows:

$$\Delta E_{CP} = E_0(\text{Complex}) - E_0(\text{NANs}) - E_0(\text{Gas})$$

where E_0 refers to the electronic energy, along with the zero-point energy correction of the NANs/gas (CO₂ or N₂) complexes and the individual molecules. ΔE_{CP} is the binding energy including the correction of the basis set superposition error (BSSE) by means of the counterpoise method.^{26, 27}



Scheme 1 Synthetic route to NANs.

Results and discussion

The formation of NANs was verified by FTIR, Elemental analysis and CP/MAS ¹³C NMR (see ESI†). The characteristic amide N-H stretching bands were observed in the range of 3344 to 3356 cm⁻¹ in the FTIR spectra of NANs. The band of C-H stretch in NANs appeared in the range of 2926 to 2928 and at 2852 cm⁻¹. The typical amide carbonyl C=O stretch was observed at 1653 cm⁻¹ for NAN-1 and NAN-2 while NAN-3 showed the appearance of C=O stretching band at relatively higher wavenumber, 1688 cm⁻¹ illustrating less conjugation and hydrogen bonding within the framework as compared to NAN-1 and NAN-2, owing to the presence of more bulky cycloaliphatic adamantane units in the structure respectively (Figure S1†). Elemental analysis further validated the successful formation of amide networks and the calculated chemical compositions of NANs are also in good agreement with the measured values. The CP/MAS ¹³C NMR spectra of NANs showed carbonyl signals in the range 160.9 ppm to 166.1 ppm respectively (Figure S2†). The peaks in the range of 125 to 153.7 ppm are attributed to the aromatic carbons of phenyl rings in the amide networks, while the chemical shifts at 38.4 to 38.9 and 45.5 to 47.5 ppm are ascribed to secondary and tertiary carbon atoms of adamantane in NANs respectively.

Powder X-ray diffraction (PXRD) of NANs reveals broad patterns suggesting amorphous nature of all amide networks due to the lack of long range order similar to the previously reported tetraphenyladamantane based porous polymer networks^{18a, 28} (Figure 1A). All NANs show a broad maxima and a shoulder in the X-ray diffractograms. The broad band around 2θ ~ 20° probably signifies the segmental distance within the polymer networks whereas the shoulder around 2θ ~ 42° is perhaps may be due to π-π stacking of amide functionality and phenyl rings in the ordered domains.²⁹ Thermal stability of adsorbents is an imperative factor for finding possible application in post combustion processes at higher temperatures and CO₂ scrubbing operations.³⁰ Keeping in view this crucial aspect, thermal stability of NANs was recorded using thermogravimetric analysis (TGA) under nitrogen atmosphere (Figure 1B). NAN-1 and NAN-2 amide networks are thermally very stable and show the decomposition above 500°C which is considerably beyond the lowest thermal stability limit for a CO₂ cyclic operation (min. 200°C).³¹ The incredible stability of these NANs is ascribed to the covalent linkages, presence of heat resistant amide groups and aromatic units in the chemical structure that increases the durability of these materials for gas separation.¹³

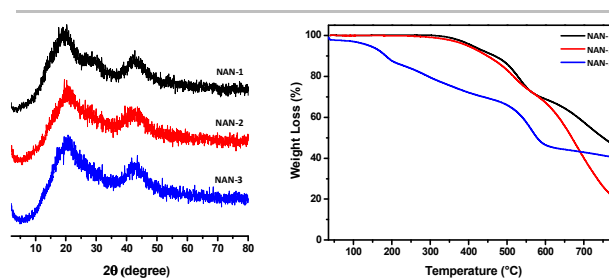


Fig. 1 (A) PXRD patterns of NANs (B) TGA curves of NANs.

On the contrary, NAN-3 show less thermal stability compared to NAN-1 and NAN-2 owing to the introduction of more cycloaliphatic adamantane units in the network that may reduce the degree of crosslinking leading to more flaws in the structure, where the initial weight loss is due to the entrapped solvent and moisture in the pores. The surface morphology of NANs was examined using scanning electron microscopy (SEM). NAN-1 image display the presence of agglomerated spherical particles¹³ in contrast to NAN-2 which shows relatively uniform and interconnected particulate structure. NAN-3 reveals the formation of granulated structure with interconnected grains forming larger particles at micro scale. Such sized particles are frequently used for fluidized bed adsorption applications at industrial level (Figure 2A-C). High-resolution transmission electron microscopy (HR-TEM) images of amide networks exhibit continuous, interconnected and extended porous network structures (Figure 2D-F).³² It is established that the formation of strong hydrogen bonds in amide polymers promotes extended three dimensional architectures.¹²

The porosity of NANs was determined using N₂ adsorption-desorption isotherms measured at 77K (Figure 3). Amide networks illustrate a typical reversible sorption isotherm. NAN-3 possesses relatively higher surface area (S_{BET} : 85 m²/g) as compared to NAN-1 and NAN-2 (Table 1, Figure S3†) and other amide functionalized porous organic polymers,^{13,14} owing to the inherent porosity generated from both the monomers having tetrahedral tecton thus forming a giant extended structure. Low surface area of NAN-1 and NAN-2 may also be due to the random orientation of pores in the network. Appearance of narrow hysteresis and pore size distribution of NANs signifies the presence of mesopores in the networks. No considerable N₂ uptake into micropores was noticed for NANs. However, at higher relative pressures, some uptake was observed illustrating existence of interparticle void spaces which is also evident from SEM micrographs (Figure 2 A-C).⁹

CO₂ and N₂ adsorption-desorption isotherms of NANs were investigated at 273K and 298K (Figure 4 and Figure 5). Among all amide networks, NAN-2 reveals the highest CO₂ sorption capacity of 65.58 mg/g followed by NAN-1 (55.78 mg/g) and NAN-3 (40.27 mg/g) at 1 bar and 273K respectively. These values for CO₂ uptake are much higher than for other porous amide polymers reported in literature.^{12, 14, 33} The CO₂ uptake of NANs at 298 K are apparently lower than the values at 273 K illustrating the exothermic nature of

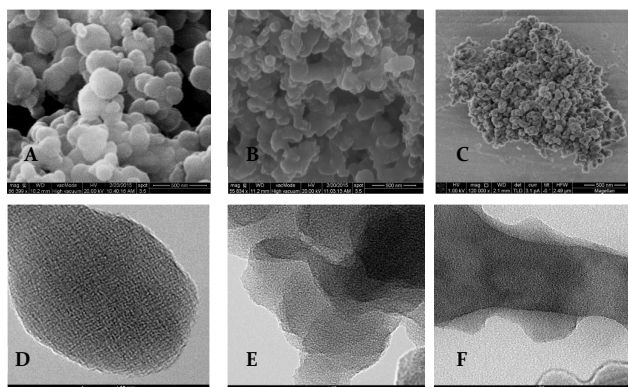


Fig. 2 SEM images of NAN-1 (A), NAN-2 (B) and NAN-3 (C). HR-TEM images of NAN-1 (D), NAN-2 (E) and NAN-3 (F)

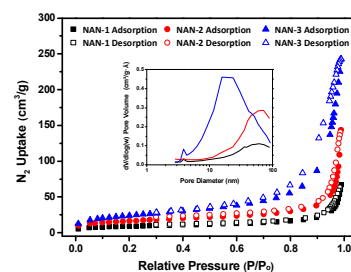


Fig. 3 N₂ gas isotherms for NANs measured at 77K (Inset: Differential pore size distribution curves from BJH method).

adsorption (Table 1).¹² To determine the sorption profile of any sorbent at 298K is very crucial because it is closer to the conditions required for post-combustion CO₂ capture³⁴ especially from the practical application perspective.³⁵ Apparently, surface area of NAN-3 is superior than NAN-1 and NAN-2 but surprisingly its CO₂ sorption capacity is the lowest of all NANs suggesting that CO₂ sorption performance of sorbents not only depends on the surface area and porosity²⁰ but also influenced by the presence of nitrogen and oxygen rich CO₂-philic groups.^{36,37} Interestingly, the polar –CONH– amide functionality is the key unit in all amide networks which is interacting with CO₂ and NAN-3 possesses less amide groups in the network relative to NAN-1 and NAN-2. Additionally, NAN-3 network contains large number of bulky adamantane moieties that create hindrance for CO₂ molecules to interact with amide groups present in the network. On the contrary, the presence of small phenyl rings in NAN-1 and NAN-2 facilitates the CO₂ molecules to approach the amide groups easily for interaction. The narrow hysteresis of adsorption-desorption curves imply weak interactions between CO₂ molecules and NANs thus allowing less energy intensive adsorbent regeneration.³⁸

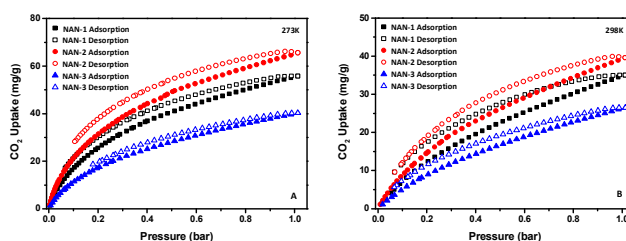


Fig. 4 CO₂ gas adsorption-desorption isotherms of NANs at (A) 273K and (B) 298K.

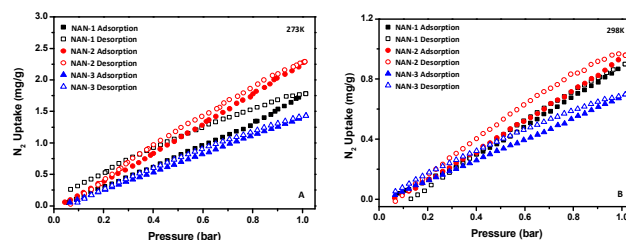
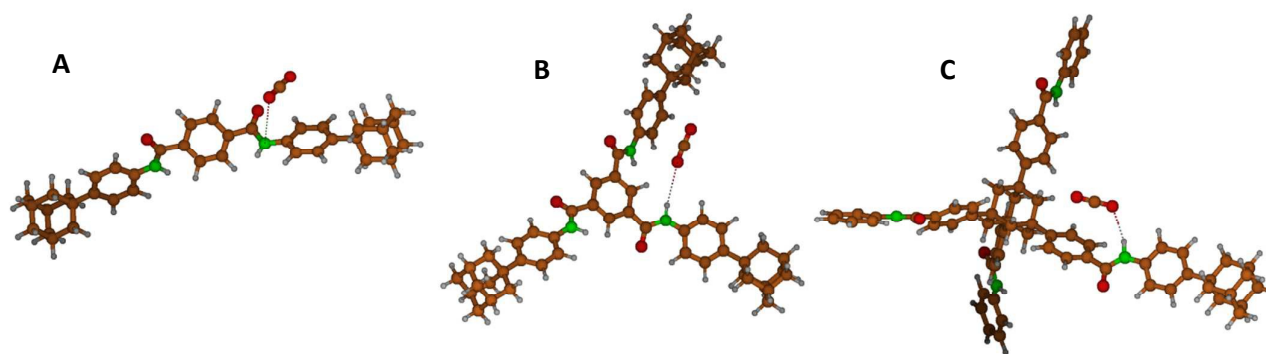


Fig. 5 N₂ gas adsorption-desorption isotherms of NANs at (A) 273K and (B) 298K.

Table 1 Surface area, pore size, CO₂ and N₂ adsorption data at 1 bar, Isothermic heat of adsorption (Q_{st}) and CO₂/N₂ selectivity of NANs.

NANs	SA _{BET} (m ² /g)	SA _{Langmuir} (m ² /g)	Pore size (nm)	CO ₂ Uptake (mg/g)		Q_{st, CO_2} (kJ/mol)	N ₂ Uptake (mg/g)		Q_{st, N_2} (kJ/mol)	CO ₂ /N ₂ Selectivity	
				T = 273K	T = 298K		T = 273K	T = 298K		T = 273K	T = 298K
NAN-1	30	47	18.9	55.78	35.02	27.94	1.78	0.89	12.32	74.0	56.4
NAN-2	56	87	22.7	65.58	39.57	31.52	2.28	0.96	21.77	72.7	66.2
NAN-3	85	135	16.2	40.27	26.49	22.46	1.43	0.69	18.55	57.8	50.1

BET and Langmuir surface area from N₂ adsorption isotherms, Average pore size from BJH adsorption, Isothermic heat of adsorption (Q_{st}) obtained from CO₂ and N₂ isotherms data at 273K and 298K using Clausius-Clapeyron equation, CO₂/N₂ selectivity calculated by IAST method for CO₂:N₂ gas mixture of 0.15:0.85.

**Fig. 6** Molecular models for (A) NAN-1/CO₂, (B) NAN-2/CO₂ and (C) NAN-3/CO₂ complexes.

Theoretical calculations were also carried out to verify our experimental findings of CO₂ capture ability of NANs. In order to calculate the interaction of a CO₂ molecule with NANs, three models have been defined for NAN-1, NAN-2 and NAN-3 (Figure 6). The results of quantum chemical calculations and geometrical parameters of CO₂ molecule in the complexes are presented in Table 2 (see Table S1 to S4 for more details †). It is observed that the binding energy of CO₂ with NAN-2 (-16.19 kJ/mol) is greater than the corresponding NAN-1 (-14.72 kJ/mol) and NAN-3 (-13.36 kJ/mol), implying that NAN-2 exhibits the highest affinity for CO₂, supporting the experimental results. The interaction takes place mainly in the region of the polar -CONH- amide groups, as it was expected.³² The magnitude of this interaction with the three models of NANs is reflected in the deviation from the linear geometry of CO₂ and in the stretching of C=O bond as well. In NAN-1-CO₂ complex, the CO₂ molecule locates in a parallel plane over the amide moiety of NAN-1 (Figure 6) at around 3.07 Å from the carbonyl oxygen and 3.40 Å from the nitrogen. Since the interaction is weak, the C=O bond lengths remain almost unchanged compared to the CO₂ free molecule (R = 1.165 Å) and the O=C=O angle deviates slightly from linearity (177.7°). In case of NAN-2-CO₂ complex, the CO₂ molecule locates along the -N-H bond line at 2.91 Å (Figure 6). Besides, the molecular structure of NAN-2, the presence of a second amide moiety located at around 3.27 Å provides an extra

stabilization of the complex. Thus, the C=O bond which interacts with the amide hydrogen is stretched (1.169 Å vs 1.165 Å of free

CO₂) and the other one is shortened (1.161 Å). As in the previous complex, the bond angle is hardly modified (178.3°). Finally, regarding NAN-3-CO₂ complex, the CO₂ molecule is located a bit farther from the amide moiety, at 3.26 Å from the nitrogen and 4.98 Å from the carbonyl oxygen, approximately (Figure 6). In this model, the extra stabilization accomplished by a second amide moiety, as in NAN-2, is absent, so that the binding energy is very similar to the one of NAN-1. Although the interaction with CO₂ in this model is slightly weaker than in NAN-1 (-13.36 vs -14.72 kJ/mol), the particular arrangement of CO₂ with respect to the amide moiety makes the geometry of this molecule to be slightly more distorted. Thus, in NAN-1 the CO₂ is located in a parallel plane and the bond lengths are hardly modified, however, in NAN-3, CO₂ is oriented at a greater extent towards the -N-H bond, and the bond distance of the C=O bond closer to the hydrogen is stretched (1.168 Å vs 1.165 Å of free CO₂) while the other bond is shortened (1.162 Å), similar as in the NAN-2 model. The bond angle, nevertheless, remains almost unchanged (179.0°). Likewise, N₂ uptake of NANs also follows the decreasing order NAN-2 > NAN-1 > NAN-3 at both the temperatures (273K and 298K), but the values are negligible relative to CO₂ uptake owing to weak interaction of NANs with N₂ which was further validated by our quantum chemical calculations (Table 2, Figure S4†). In NAN-1, the interaction takes place mainly

Paper

Journal of Materials Chemistry A

with the aromatic ring, and the N₂ locates on a plane parallel over it, whereas in NAN-2, the interaction is similar as in the case of CO₂, and two amide groups stabilizes the N₂ and higher affinity is

Table 2 Binding energy of CO₂ and N₂ with NANs (ΔE_{CP}), in kJ/mol, C=O bond length (R_1), in Å, and O=C=O angle (α), in degrees, of the CO₂ molecule, N=N bond length (R), in Å. Data obtained at the ω B97XD/6-31+G(d,p)// ω B97XD/6-311++G(2df,2p) level of theory.

NANs	CO ₂			N ₂		
	ΔE_{CP}	R_1	R_2	α	ΔE_{CP}	R
NAN-1	-14.72	1.166	1.164	177.7	-6.68	1.102
NAN-2	-16.19	1.169	1.161	178.3	-10.33	1.102
NAN-3	-13.36	1.168	1.168	179.0	-6.49	1.102

observed. While similar to CO₂, N₂ locates over the benzene ring and the extra stabilization of the second amide is absent in NAN-3 (Figure S4†).

Isosteric heat of adsorption (Q_{st,CO_2}) was calculated to determine the binding affinity between NANs and CO₂ molecules from the CO₂ adsorption isotherms measured at 273K and 298K using Clausius-Clapeyron equation (Figure 7A). This parameter performs a key role in determining the adsorption selectivity and energy required for CO₂ release during regeneration phase. Q_{st,CO_2} for NANs are in the range of 22.46 – 31.52 kJ/mol which is distinctly less than expected for chemisorption (> 40 kJ/mol), signifying a physisorption process similar to other porous polymers.³⁶ Q_{st,CO_2} values exhibit a noticeable decreasing trend with the adsorbed amount of CO₂, suggesting strong interactions of the polarizable CO₂ molecules through dipole-quadrupole interactions with the polar amide groups in NANs rather than the gas-gas interaction and aggregation of the CO₂ molecules themselves. Isosteric heat of N₂ adsorption for NANs (Q_{st,N_2}) was also calculated and values appeared in the physisorption range (Figure S5†).

High selectivity of CO₂ over N₂ is one of the essential features for an adsorbent to be exploited for post-combustion CO₂ capture. The foremost concern in CO₂/N₂ gas separation is the minute difference in properties of both the gases which is clear from the kinetic diameters of CO₂ (3.30 Å), and N₂ (3.64 Å). Conversely, their quadrupole moments and polarizabilities exhibit some differences, where CO₂ possesses a large quadrupole moment of 13.4×10^{-40} Cm² as compared to N₂ (4.7×10^{-40} Cm²) and a polarizability of 26.3×10^{-25} cm³ (17.6×10^{-25} cm³ for N₂). Accordingly, the variation in chemical reactivity of gases can assist control at the molecular level resulting in strong interactions of the sorbents with the surface of pores and increased selectivity.³⁹ In addition to high CO₂ uptake, high CO₂/N₂ selectivity of adsorbents is equally crucial from practical application perspective. To evaluate the performance of NANs in CO₂ separation from gas mixtures, Ideal Adsorbed Solution Theory (IAST) was used (Table S5 and Figure S6†). For this purpose, CO₂ and N₂ single component isotherms were fitted by Langmuir dual sites or Langmuir single site models to calculate CO₂/N₂ selectivity by IAST method for CO₂:N₂ binary gas mixture

containing 15% CO₂ and 85% N₂, a typical post-combustion flue gas composition. The CO₂/N₂ selectivity of NAN-1, NAN-2 and NAN-3 at 1 bar is 74.0, 72.7 and 57.8 at 273K and 56.4, 66.2 and 50.1 at

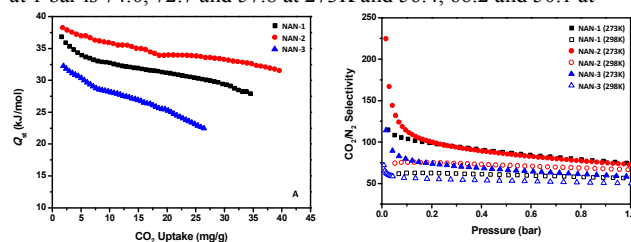


Fig. 7 (A) Isothermic heat of CO₂ adsorption for NANs. (B) CO₂/N₂ selectivity calculated by IAST method for CO₂:N₂ gas mixture of 0.15:0.85.

298K respectively (Table 1 and Figure 7B). Keeping in view the conditions required for post-combustion capture, it is imperative to determine CO₂/N₂ selectivity at 298K while some studies were only focused on 273K.²² These NANs display CO₂/N₂ selectivity with reasonable retention on changing temperature from 273K to 298K. Noticeably at 298K, NAN-2 performed certainly well in terms of selectivity (66.2) followed by NAN-1 and then NAN-3, duly complementing the same sequence for CO₂ uptake capacity determined through experimental as well as theoretical estimations. Interestingly, these NANs exhibit higher CO₂/N₂ selectivity, surpassing the selectivity for many porous polymers reported in literature at these temperatures^{40,41} even having much larger surface area correspondingly (Table S6†).⁴²⁻⁴⁸ The CO₂ selectivity of NANs is due to the extensive interactions between CO₂ and amide functional groups present in the networks thus, proving the superiority of using amide link in the NANs architecture.¹² In fact, the basic amide functionality possesses binary interaction sites (N-H and C=O) and a strong Lewis acid-base interaction exists between CO₂ molecules and oxygen of amide carbonyl moiety. Likewise, this interaction in NANs is evident from reasonably high CO₂ uptakes and marked CO₂/N₂ selectivities owing to the CO₂ affinity of N-containing amide groups.¹² Interestingly, mesoporosity might also be another factor responsible for this decent CO₂/N₂ selectivity together with contribution from CO₂ philic amide groups.²³ Porous polymers⁴⁹ in this respect, specially containing azo linkages have already been exploited for selective CO₂ capture.^{47,48} Another study⁵⁰ reveals that an ideal sorbent should possess high CO₂/N₂ selectivity at low CO₂ pressures (<0.2 bar) which is in good agreement with our results displaying the decreasing pattern of CO₂/N₂ selectivity with the increase in pressure owing to the pressure-driven pore-filling mechanism, irrespective of CO₂-philic moieties present in the networks (Figure 7B).

Conclusions

We presented first ever study on the nanoporous nitrogen rich amide networks based on tetraphenyladamantane using one pot facile strategy. These thermally stable NANs also possess reasonable CO₂ sorption capacity and notable CO₂/N₂ selectivity (74.0 at 273K for NAN-1). A combined impact emanating from the presence of CO₂ philic N-containing amide groups and mesoporosity in the

architectures are the key basis for this CO₂/N₂ selectivity thus, making these materials promising contenders for post-combustion CO₂ capture and real gas separation applications. These amide networks can potentially be commercialized at large scale owing to their simple and catalyst free synthetic protocol. Therefore, the current effort open up further avenues to tailor and design new thermally stable amide based sorbents for efficient gas separation.

Acknowledgments

Dr Sonia Zulfiqar is highly thankful for the financial support provided by Marie Curie IIF grant "NABPIL" (No. 629050) from the European Commission under the 7th Framework Programme (FP7-PEOPLE-2013-IIF) and also appreciate the cooperation of Dr. José Ignacio Santos for Solid State NMR facility, Iñigo Pérez Miqueo for BET measurements and Dr. Monica Moreno for administrative support from UPV/EHU, San Sebastian, Spain. The authors would like to thank for technical and human support provided by IZO-SGI SGIker of UPV/EHU and European funding (ERDF and ESF). Daniele Mantione is highly grateful for financial support provided through EU project FP7-PEOPLE-212-ITN 316832-OLIMPIA.

Notes and references

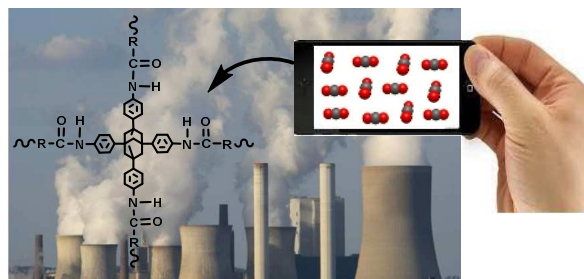
- R. A. Kerr, *Science* 2007, **316**, 188–190.
- D. M. D' Alessandro, B. Smit and J. R. Long, *Angew. Chem. Int. Ed.*, 2010, **49**, 6058–6082.
- L. Zou, D. Feng, T-F. Liu, Y-P. Chen, S. Fordham, S. Yuan, J. Tiana and H-C. Zhou, *Chem. Commun.*, 2015, **51**, 4005–4008.
- P. M. Budd, N. B. McKeown and D. Fritsch, *Macromol. Symp.*, 2006, **245–246**, 403–405.
- B. Lukose, A. Kuc and T. Heine, *Chem. Eur. J.*, 2011, **17**, 2388–2392.
- A. I. Cooper, *Adv. Mater.*, 2009, **21**, 1291–1295.
- S. Xu, Y. Luo and B. Tan, *Macromol. Rapid Commun.*, 2013, **34**, 471–484.
- R. Babarao, S. Dai and D. Jiang, *Langmuir*, 2011, **27**, 3451–3460.
- Y. Liao, J. Weber and C. F. J. Faul, *Macromolecules*, 2015, **48**, 2064–2073.
- M. U. Alvi, S. Zulfiqar, C. T. Yavuz, H-S. Kweon and M. I. Sarwar, *Ind. Eng. Chem. Res.*, 2013, **52**, 6908–6915.
- S. Zulfiqar, S. I. Shah and M. I. Sarwar, *Ind. Eng. Chem. Res.*, 2013, **52**, 11050–11060.
- S. Zulfiqar, M. I. Sarwar and C. T. Yavuz, *RSC Adv.*, 2014, **4**, 52263–52269.
- L. Rajput and R. Banerjee, *Cryst. Growth Des.*, 2014, **14**, 2729–2732.
- S. Zulfiqar, S. Awan, F. Karadas, M. Atilhan, C. T. Yavuz and M. I. Sarwar, *RSC Adv.*, 2013, **3**, 17203–17213.
- M. Bremer, P. S. Gregory and P. v. R. Schleyer, *J. Org. Chem.*, 1989, **54**, 3796–3799.
- B. Chen, M. Eddaoudi, T. Reineke, J. Kampf, M. O. Keeffe and O. M. Yaghi, *J. Am. Chem. Soc.*, 2000, **122**, 11559–11560.
- R.W. Murray, S. N. Rajadhyaksha and L. Mohan, *J. Org. Chem.*, 1989, **54**, 5783–5788.
- (a) C. Shen, H. Yu and Z. Wang, *Chem. Commun.*, 2014, **50**, 11238–11241. (b) C. Shen, Y. Bao and Z. Wang, *Chem. Commun.*, 2013, **49**, 3321–3323.
- H. Kim, M. C. Cha, H. W. Park and J. Y. Chang, *J. Polym. Sci. Part A: Polym. Chem.*, 2013, **51**, 5291–5297.
- T. Muller and S. Brase, *RSC Adv.*, 2014, **4**, 6886–6907.
- G. Li, B. Zhang and Z. Wang, *Macromol. Rapid Commun.*, 2014, **35**, 971–975.
- G. Li, B. Zhang, J. Yan and Z. Wang, *Macromolecules*, 2014, **47**, 6664–6670.
- J. H. Lee, H. J. Lee, S- Y. Lim, B. G. Kim and J.W. Choi, *J. Am. Chem. Soc.*, 2015, **137**, 7210–7216.
- Gaussian 09, Revision A.1, M. J. Frisch, G. W. Trucks, H. B. Schlegel, G. E. Scuseria, M. A. Robb, J. R. Cheeseman, G. Scalmani, V. Barone, B. Mennucci, G. A. Petersson, H. Nakatsuji, M. Caricato, X. Li, H. P. Hratchian, A. F. Izmaylov, J. Bloino, G. Zheng, J. L. Sonnenberg, M. Hada, M. Ehara, K. Toyota, R. Fukuda, J. Hasegawa, M. Ishida, T. Nakajima, Y. Honda, O. Kitao, H. Nakai, T. Vreven, Jr., J. A. Montgomery, J. E. Peralta, F. Ogliaro, M. Bearpark, J. J. Heyd, E. Brothers, K. N. Kudin, V. N. Staroverov, R. Kobayashi, J. Normand, K. Raghavachari, A. Rendell, J. C. Burant, S. S. Iyengar, J. Tomasi, M. Cossi, N. Rega, J. M. Millam, M. Klene, J. E. Knox, J. B. Cross, V. Bakken, C. Adamo, J. Jaramillo, R. Gomperts, R. E. Stratmann, O. Yazyev, A. J. Austin, R. Cammi, C. Pomelli, J. W. Ochterski, R. L. Martin, K. Morokuma, V. G. Zakrzewski, G. A. Voth, P. Salvador, J. J. Dannenberg, S. Dapprich, A. D. Daniels, Ö. Farkas, J. B. Foresman, J. V. Ortiz, J. Cioslowski and D. J. Fox, Gaussian Inc., Wallingford CT, 2009.
- J.-D. Chai and M. Head-Gordon, *Phys. Chem. Chem. Phys.*, 2008, **10**, 6615–6620.
- S. F. Boys and F. Bernardi, *Mol. Phys.*, 1970, **19**, 553–566.
- S. Simon, M. Duran and J. J. Dannenberg, *J. Chem. Phys.*, 1996, **105**, 11024–11031.
- T. Islamoglu, M. G. Rabbani and H. M. El-Kaderi, *J. Mater. Chem. A*, 2013, **1**, 10259–10266.
- E. M. Maya, I G. Yoldi, A. E. Lozano, J. G. de la Campa and J. de Abajo, *Macromolecules*, 2011, **44**, 2780–2790.
- X. Zhu, C-L. Do-Thanh, C. R. Murdock, K.M. Nelson, C. Tian, S. Brown, S. M. Mahurin, D.M. Jenkins, J. Hu, B. Zhao, H. Liu and S. Dai, *ACS Macro Lett.*, 2013, **2**, 660–663.
- D. Ko, H. A. Patel and C. T. Yavuz, *Chem. Commun.*, 2015, **51**, 2915–2917.
- V. M. Suresh, S. Bonakala, H. S. Atreya, S. Balasubramanian and T. K. Maji, *ACS Appl. Mater. Interfaces*, 2014, **6**, 4630–4637.
- S. Zulfiqar and M. I. Sarwar, *Polymer Science, Ser. B*, 2015, **57**, 702–709.
- R. Dawson, E. Stockel, J. R. Holst, D. J. Adams and A. I. Cooper, *Energy Environ. Sci.*, 2011, **4**, 4239–4245.
- M. M. Unterlass, F. Emmerling, M. Antonietti and J. Weber, *Chem. Commun.*, 2014, **50**, 430–432.
- R. Dawson, D. J. Adams and A. I. Cooper, *Chem. Sci.*, 2011, **2**, 1173–1177.
- S. Zulfiqar, F. Karadas, J. Park, E. Deniz, G. D. Stucky, Y. Jung, M. Atilhan and C. T. Yavuz, *Energy Environ. Sci.*, 2011, **4**, 4528–4531.
- M. G. Rabbani and H. M. El-Kaderi, *Chem. Mater.*, 2011, **23**, 1650–1653.
- S. Zulfiqar, M. I. Sarwar and Mecerreyes, D. *Polym. Chem.*, 2015, **6**, 6435–6451.
- H.A. Patel, D. Ko and C. T. Yavuz, *Chem. Mater.*, 2014, **26**, 6729–6733.
- S. Hug, M. B. Mesch, H. Oh, N. Popp, M. Hirscher, J. Senker and B. V. Lotsch, *J. Mater. Chem. A*, 2014, **2**, 5928–5936.
- A. K. Sekizkardes, S. Altarawneh, Z. Kahveci, T. Islamoğlu and H. M. El-Kaderi, *Macromolecules*, 2014, **47**, 8328–8334.
- W-C. Song, X-K. Xu, Q.Chen, Z-Z. Zhuang and X-H. Bu, *Polym. Chem.*, 2013, **4**, 4690–4696.
- S. Ren, M J. Bojdy, R. Dawson, A. Laybourn, Y. Z. Khimyak, D. J. Adams and A. I. Cooper, *Adv. Mater.*, 2012, **24**, 2357–2361.
- M. R. Liebl and J. Senker, *Chem. Mater.*, 2013, **25**, 970–980.
- S. Xiong, X. Fu, L. Xiang, G. Yu, J. Guan, Z. Wang, Y. Du, X. Xiong and C. Pan, *Polym. Chem.*, 2014, **5**, 3424–3431.

Paper

Journal of Materials Chemistry A

- 47 P. Arab, M. G. Rabbani, A. K. Sekizkardes, T. Islamoglu and H. M. El-Kaderi, *Chem. Mater.*, 2014, **26**, 1385–1392.
- 48 J. Lu and J. Zhang, *J. Mater. Chem. A* 2014, **2**, 13831–13834.
- 49 E. Merino, E. Verde-Sesto, E. M. Maya, M. Iglesias, F. Sanchez and A. Corma, *Chem. Mater.*, 2013, **25**, 981–988.
- 50 G. Liu, Y. Wang, C. Shen, Z. Ju and D. Yuan, *J. Mater. Chem. A*, 2015, **3**, 3051–3058.

Table of Contents



This paper reveals the potential of nanoporous amide networks based on tetraphenyladamantane for selective CO₂ capture